Supplemental Material

Accurate HER2 determination in breast cancer: A prominent COF-immobilized enzyme-enhanced electrochemical aptasensor employing 4-acetamidophenol as an efficient mediator

Yue Zhang[1*], Shuyi Chen[1], Jie Ma[2], Xiaobin Zhou[1], Xinchen Sun[1], Chenglin Zhou[1*]

[1]Clinical Medical Laboratory Center, Gaogang Branch, Taizhou School of Clinical Medicine, Nanjing Medical University, The Affiliated Taizhou People's Hospital of Nanjing Medical University, Taizhou 225300, China

[2]Clinical laboratory department, The Second Affiliated Hospital of Anhui Medical University, Hefei 230601, China

[*]Address correspondence to: Yue Zhang; yue_zhang@aa.seu.edu.cn and Chenglin Zhou; 18762340015@njmu.edu.cn.

Experimental section

Apparatus

Transmission electron microscopy (TEM) iamges and high-resolution transmission electron micrographs (HRTEM) images were recorded on a FEI talos F200x G2 transmission electron microscope (Thermo Scientific, USA). UV-visible absorption spectra (UV-vis) were taken on a UV-3600i Plus spectrophotometer (Shimadzu, Japan). Fourier transform infrared spectra (FT-IR) were performed on a Nicolet iS20 infrared spectrometer (Thermo Scientific, USA). X-ray diffractometer (XRD) was conducted via a SmartLab 9kW X-ray diffractometer (Rigaku, Japan). X-ray photoelectron spectroscopy (XPS) was collected with a K-Alpha X-ray photoelectron spectrometer (Thermo Scientific, USA). Brunauer-Emmett-Teller (BET) surface area and pore volume were carried out with an ASAP 2460 analyzer (Micromeritics, USA). Thermogravimetric analysis (TGA) was conducted on the STA 499 F5 Jupiter synchronous thermal analyzer (Netzsch, Germany) in the nitrogen atmosphere. All electrochemical measurements were implemented utilizing a CHI660E electrochemical workstation with a three-electrode system (Chenhua Instruments, China). The glassy carbon electrode (GCE) or Pt ultramicroelectrode, a platinum wire, and an Ag/AgCl (3 M KCl) electrode (Chenhua Instruments, China) were employed as the working, counter, and reference electrodes, respectively. The kinetics study and stability of enzyme were measured with an Epoch full-wavelength microplate reader (BioTek, USA). CEA and CA15-3 were tested by using ARCHITECT i2000SR immunoassay analyzer (Abbott, USA).

Immobilization efficiency analysis

Following antibody conjugation to the AuNPs@COF, the resulting precipitate was collected through centrifugation, washed, and resuspended in PBS. HRP was then added, allowed to react, and the supernatant collected by centrifugation. The concentration of unimmobilized HRP in the supernatant was measured utilizing a BCA protein assay kit (Beyotime). Immobilization efficiency was calculated based on the ratio of unimmobilized HRP to the total HRP added. The BCA assay was performed according to the manufacturer's instructions. Briefly, 20 μL of protein standards or samples were added to a 96-well plate, followed by 200 μL of BCA working solution. After incubation at 37°C for 30 minutes, absorbance at 562 nm was measured with a microplate reader, and sample concentrations were determined from a standard curve. The quantity of unimmobilized HRP was calculated from the supernatant volume, from which the immobilization efficiency was calculated.

Surface plasmon resonance (SPR) assay

The in-tandem SPR assay was carried out on a BIAcore T200 instrument (GE Healthcare) with a CM5 sensor chip at 25 °C, following the manufacturer's guidelines. The process involved mixing 50 μL of HER2 protein with 10 mM sodium acetate solution (pH 5.0) and immobilizing it on the CM5 sensor chip's flow cell through amine coupling. Then, any remaining activation groups were blocked utilizing 1 M ethanolamine (pH 8.5). A reference aisle experienced similar activation and blocking, but with PBS (pH 5.0). To appraise the binding site profiles, we first introduced 5 nM of aptamer into the flow cell utilizing phosphate-buffered saline (PBS-P+ buffer)

containing descaler (pH 7.4) at a flow rate of 30 μL min^{-1}, allowing 120 s for binding. Once the aptamer reached saturation in HER2 binding, 2 nM of either aptamer or antibody was injected again, permitting another 120 s of binding. The comparison of response units between the second-injected aptamer and antibody allowed us to determine whether they bind to different sites on HER2. We collected sample-related data utilizing BIAcore T200 Control software (version 2.0, GE Healthcare).

Cell culture

MDA-MB-231 cells were maintained in complete L-15 medium, MCF-7 cells in complete MEM medium, and ZR-75-1 cells in RPMI-1640 medium supplemented with 10% FBS and 1% penicillin-streptomycin. MCF-10A cells were cultured in a specialized breast epithelial cell medium. All cell lines were incubated at 37℃ in a 5% CO_2 atmosphere. For subculturing, cells were detached with a 0.25% trypsin-EDTA solution, harvested by centrifugation, and resuspended in fresh media. To evaluate HER2 levels in cell culture supernatants, cells were incubated in the 12-well plate with 2×10^5 cells mL^{-1} per well for 24 h. The supernatants were then collected for analysis. Cell lines and cell culture reagents were purchased from Shanghai Whelab Bioscience Co., Ltd.

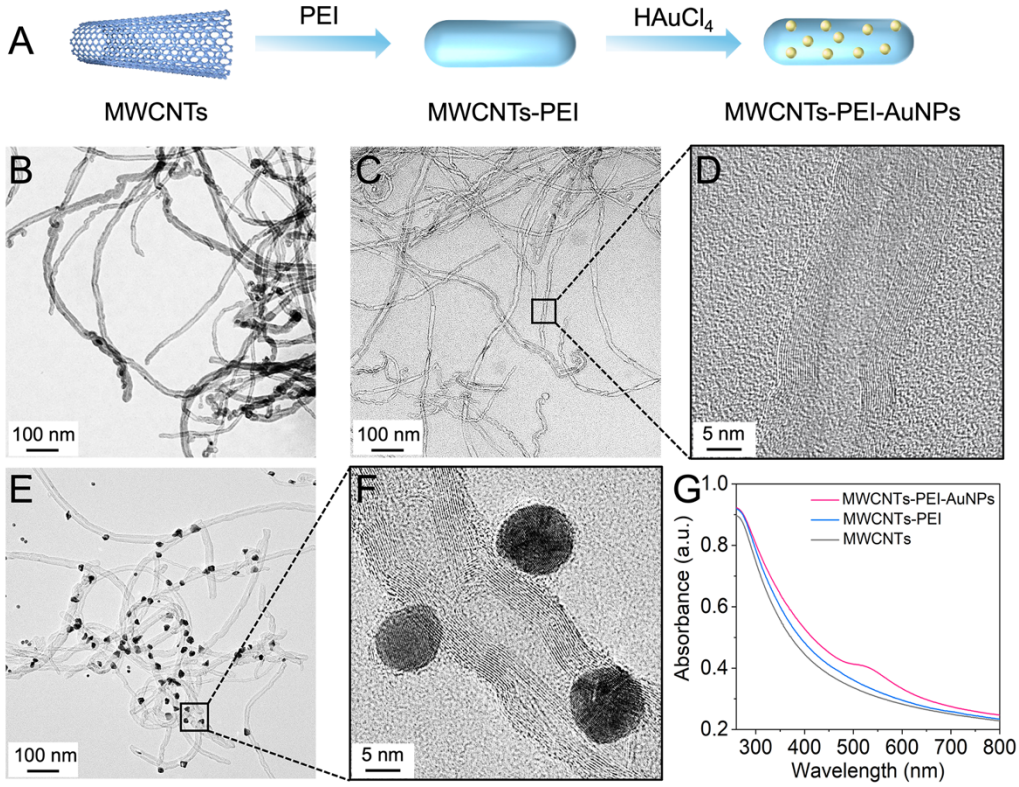

Fig. S1 (A) Schematic of synthesis process of MWCNTs-PEI-AuNPs. TEM images of (B) MWCNTs, (C) MWCNTs-PEI, and (E) MWCNTs-PEI-AuNPs. HRTEM images of (D) MWCNTs-PEI and (F) MWCNTs-PEI-AuNPs. (G) UV-vis absorption spectra of MWCNTs, MWCNTs-PEI, and MWCNTs-PEI-AuNPs.

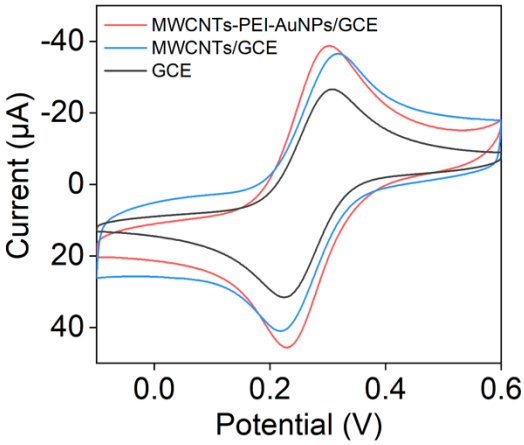

Fig. S2 CV curves of different modified GCE electrodes in 0.1 M PBS (pH 7.4) containing 2 mM $K_3Fe(CN)_6$.

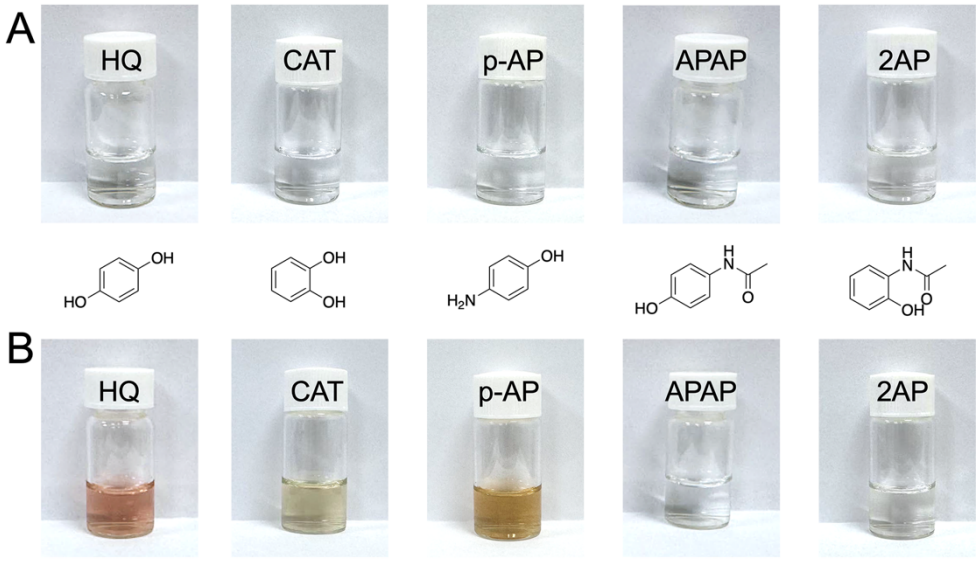

Fig. S3 Photographs of HQ, CAT, p-AP, APAP, and 2AP dissolved in 0.1 M PBS (pH 7.4) at room temperature without light protection (A) before and (B) after 1 h, respectively.

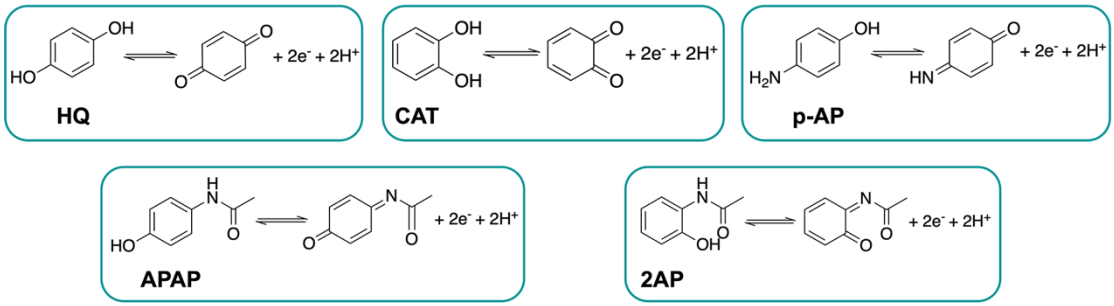

Fig. S4 Electron transfer mechanisms of HQ and candidate mediators.

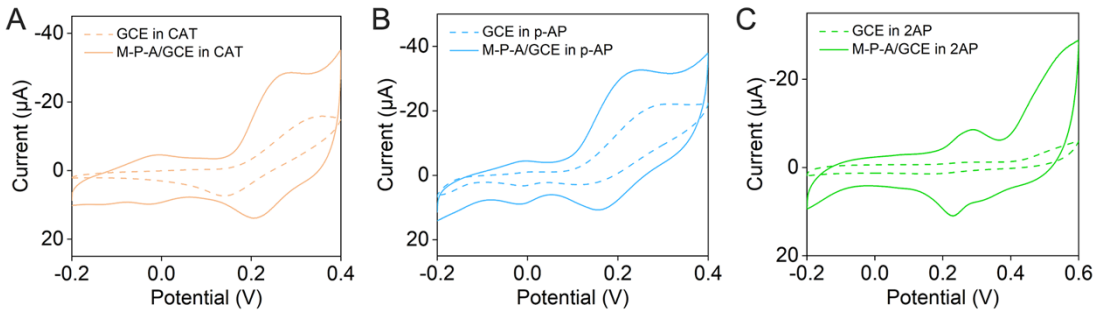

Fig. S5 CV responses obtained using MWCNTs-PEI-AuNPs modified- or bare GCE electrodes in 0.1 M PBS (pH 7.4) containing 2 mM (A) CAT, (B) p-AP, and (C) 2AP.

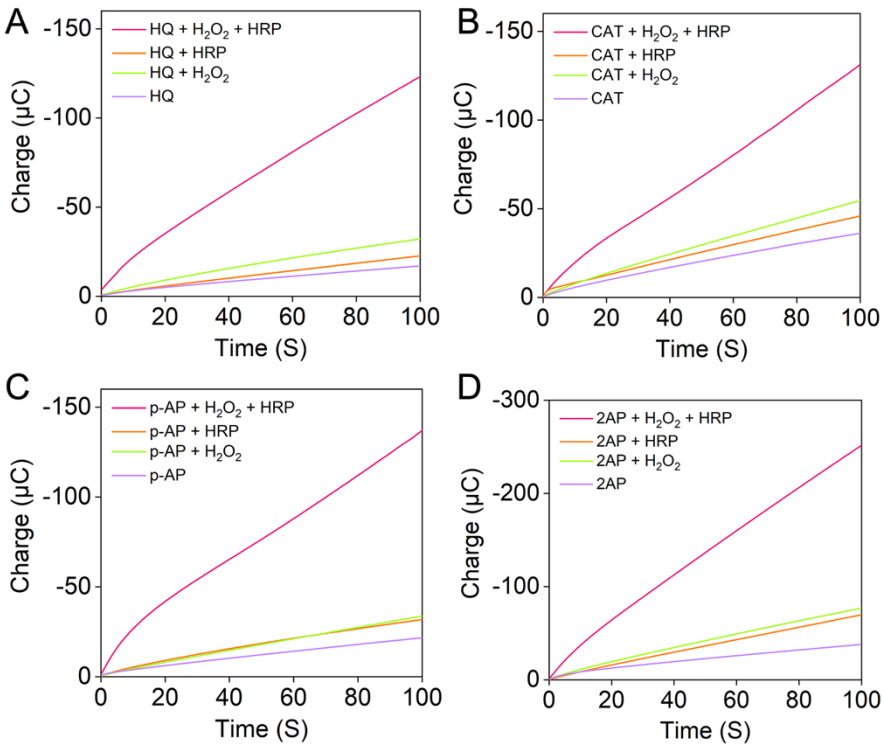

Fig. S6 Chronocoulograms obtained using GCE electrodes at 0.0 V in (A) 0.1 M PBS (pH 7.4) containing 2 mM HQ, PBS containing 2 mM HQ and 3 mM H_2O_2, PBS containing 2 mM HQ and 40 μg mL^{-1} HRP, and PBS containing 2 mM HQ, 3 mM H_2O_2 and 40 μg mL^{-1} HRP, (B) 0.1 M PBS (pH 7.4) containing 2 mM CAT, PBS containing 2 mM CAT and 3 mM H_2O_2, PBS containing 2 mM CAT and 40 μg mL^{-1} HRP, and PBS containing 2 mM CAT, 3 mM H_2O_2 and 40 μg mL^{-1} HRP, (C) 0.1 M PBS (pH 7.4) containing 2 mM p-AP, PBS containing 2 mM p-AP and 3 mM H_2O_2, PBS containing 2 mM p-AP and 40 μg mL^{-1} HRP, and PBS containing 2 mM p-AP, 3 mM H_2O_2 and 40 μg mL^{-1} HRP, (D) 0.1 M PBS (pH 7.4) containing 2 mM 2AP, PBS containing 2 mM 2AP and 3 mM H_2O_2, PBS containing 2 mM 2AP and 40 μg mL^{-1} HRP, and PBS containing 2 mM 2AP, 3 mM H_2O_2 and 40 μg mL^{-1} HRP.

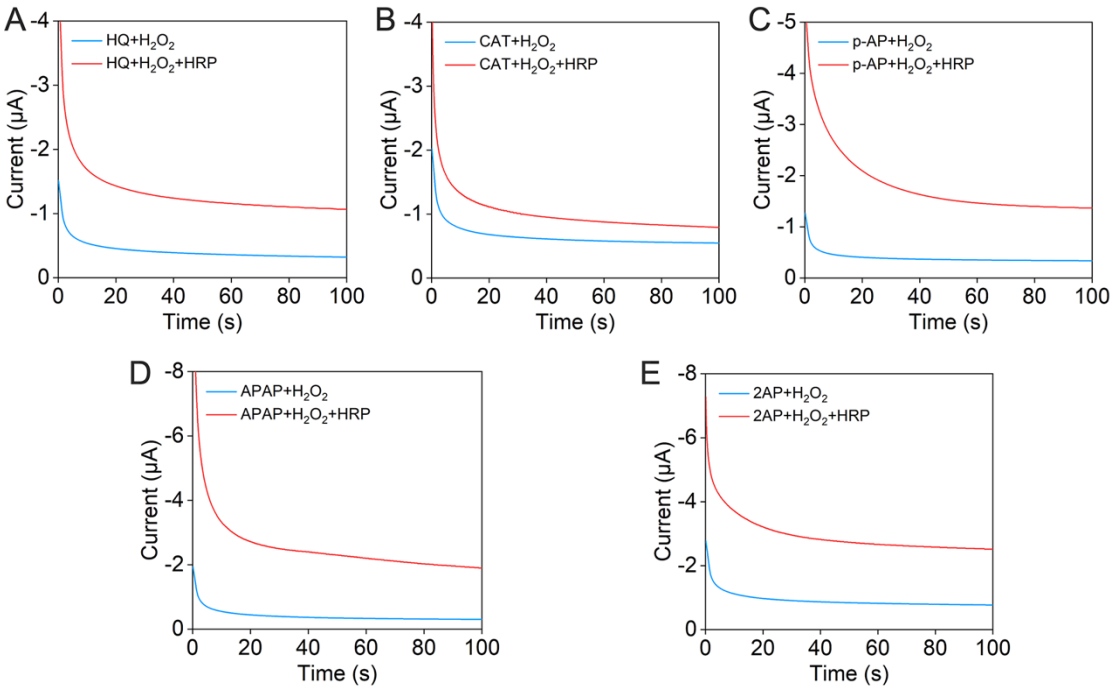

Fig. S7 Chronoamperograms obtained using GCE electrodes (diameter = 3 mm) at 0.0 V in (A) 0.1 M PBS (pH 7.4) containing 2 mM HQ and 3 mM H_2O_2, PBS containing 2 mM HQ, 3 mM H_2O_2 and 40 μg mL^{-1} HRP, (B) 0.1 M PBS (pH 7.4) containing 2 mM CAT and 3 mM H_2O_2, PBS containing 2 mM CAT, 3 mM H_2O_2 and 40 μg mL^{-1} HRP, (C) 0.1 M PBS (pH 7.4) containing 2 mM p-AP and 3 mM H_2O_2, PBS containing 2 mM p-AP, 3 mM H_2O_2 and 40 μg mL^{-1} HRP, (D) 0.1 M PBS (pH 7.4) containing 2 mM APAP and 3 mM H_2O_2, PBS containing 2 mM APAP, 3 mM H_2O_2 and 40 μg mL^{-1} HRP, (E) 0.1 M PBS (pH 7.4) containing 2 mM 2AP and 3 mM H_2O_2, PBS containing 2 mM 2AP, 3 mM H_2O_2 and 40 μg mL^{-1} HRP. I_{lim} was obtained using the absolute current value of the blue curve subtracted from the absolute current value of the red curve at 50 s.

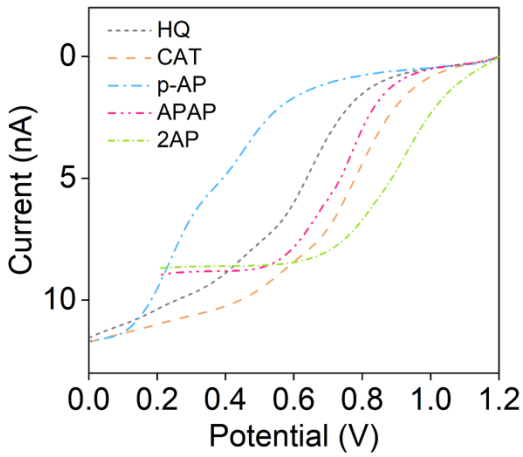

Fig. S8 Linear sweep voltammetric curves obtained using Pt ultramicroelectrodes (diameter = 10 μm) in 0.1 M PBS (pH 7.4) containing 2 mM HQ, CAT, p-AP, APAP, and 2AP.

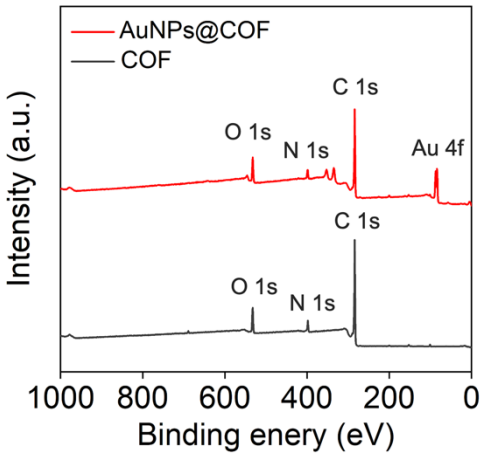

Fig. S9 XPS full-spectrum scan of COF and AuNPs@COF.

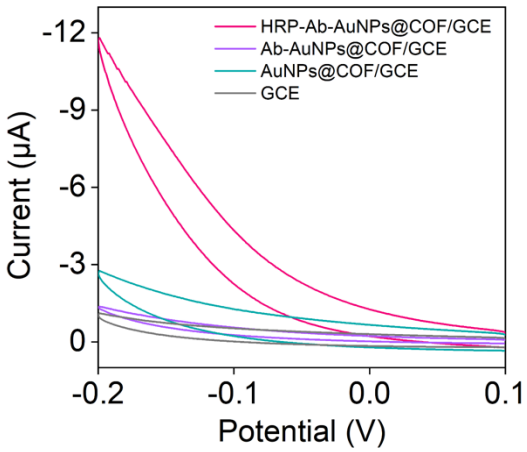

Fig. S10 CV of different modified GCE electrodes in 0.1 M PBS (pH 7.4) containing 2 mM APAP and 3 mM H_2O_2.

Table S1. Enzyme loading and immobilization efficiency on the COF complex.

Enzyme	Total amount of enzyme added (mg)	Enzyme remaining in the supernatant (mg)	Enzyme loading (mg)	Immobilization Efficiency (%)
HRP	1	0.177	0.823	82.3

The loading amount and immobilization efficiency of HRP on the COF complex were calculated from the difference in enzyme concentration in solution before and after immobilization, as presented in Table S1. The immobilization efficiency of HRP on the COF complex was determined to be 82.3%. Comparisons of the performance of free and immobilized enzymes in subsequent experiments were based on this immobilization efficiency, ensuring equivalent amounts of HRP.

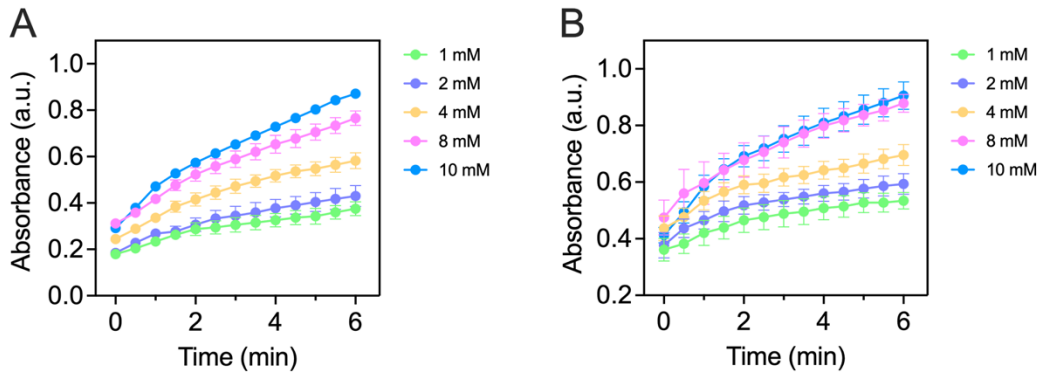

Fig. S11 Absorbance at 652 nm as the result of oxTMB generation in the presence of (A) free HRP and (B) HRP-Ab-AuNPs@COF with different concentrations of H_2O_2.

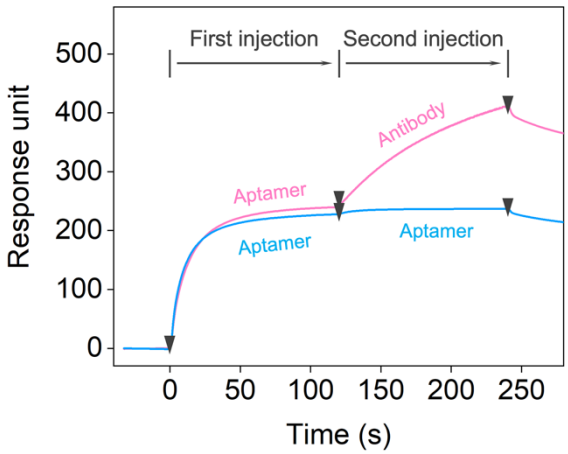

Fig. S12 SPR measurements of HER2 binding sites of the aptamer and antibody. HER2 proteins were immobilized onto the CM5 sensor chips. The antibody or aptamer was injected again after the aptamer reached saturation in HER2 binding.

To analyze the binding sites of the aptamer and antibody against HER2, HER2 proteins were immobilized on the CM5 chip, and in-tandem SPR was utilized to verify whether the antibody could bind to HER2 when aptamer binding sites were saturated. As presented in Fig. S12, the response signal remained constant (blue line) with continued aptamer addition after saturation, while the response signal increased significantly (pink line) with continued antibody addition, indicating that the aptamer and the antibody targeted different HER2 binding sites without competitive interaction. Therefore, the aptamer and the antibody were perfectly suitable for the construction of HER2 aptasensor.

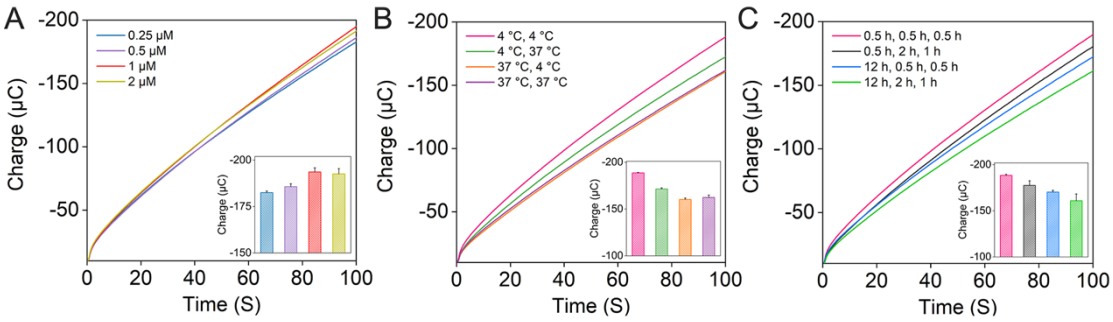

Fig. S13 Chronocoulograms obtained at 0.0 V for the aptasensors fabricated with (A) different HER2 aptamer concentrations, (B) different incubation temperatures for HER2 and HRP-Ab-AuNPs@COF, and (C) different incubation times for HER2 aptamer, HER2 and HRP-Ab-AuNPs@COF in 0.1 M PBS (pH 7.4) containing 2 mM APAP and 3 mM H_2O_2. Insets: Histograms showed the statistical results of the corresponding chronocoulograms.

Table S2. Comparison of the analytical performance of the reported HER2 biosensors constructed using different methods.

Detection methods	Linear range (ng mL^{-1})	LOD (pg mL^{-1})	Ref.
Electrochemiluminescence biosensor	0.01-500	6.65	[1]
MNA-based electrochemical immunosensor	10-250	4800	[2]
Ratiometric electrochemical immunosensor	0.01-100	3.3	[3]
Label-free electrochemical biosensor	0.1-100	500	[4]
Nanozyme-based electrochemical immunosensor	0.01-10	5.4	[5]
Smartphone-based photoelectrochemical immunoassay	0.01-10	3.5	[6]
Antifouling electrochemical biosensor	0.1-1000	45	[7]
Nanozyme-based electrochemical immunoassay	0.01-50	4.5	[8]
Immobilized enzyme-enhanced electrochemical aptasensor	0.0005-100	0.418	This work

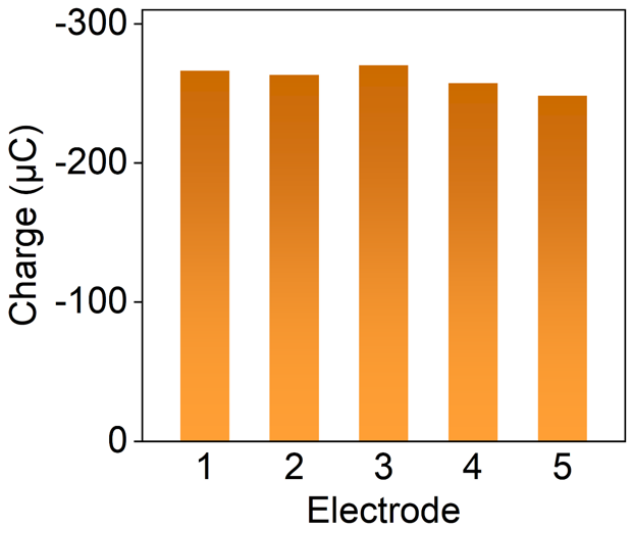

Fig. S14 Charge values of five individual aptasensors for HER2 with a concentration of 1 ng mL^{-1}.

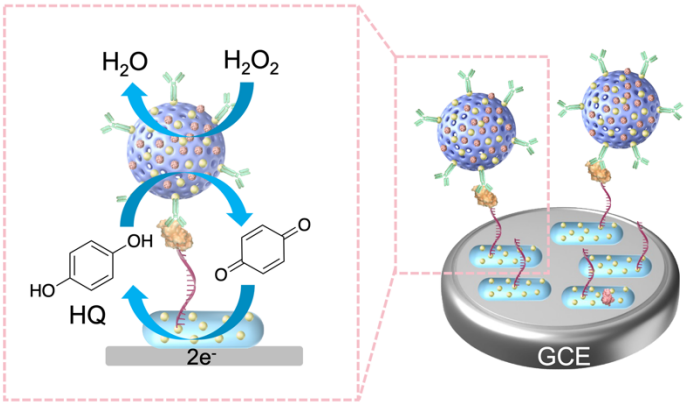

Fig. S15 Schematic of detection mechanism of HQ-mediated system.

Table S3. Recovery test of HER2 in actual healthy human serum.

Sample	Standard value (ng mL^{-1})	Found (ng mL^{-1})	Recovery (%)	RSD (n = 3) (%)
1	10	9.110	91.104	7.531
2	0.1	0.098	98.403	1.096
3	0.001	0.001	102.925	6.200

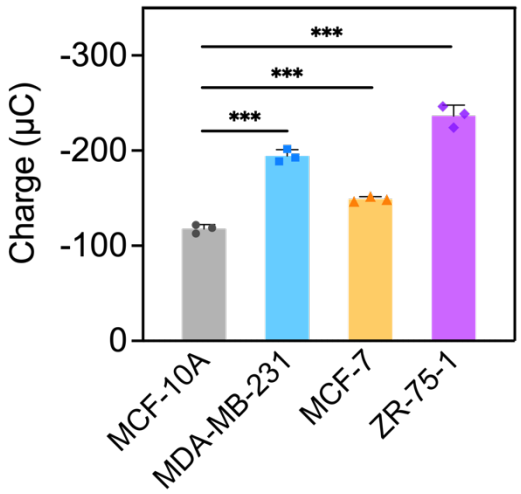

Fig. S16 HER2 levels in culture supernatants from different cell lines measured using the proposed aptasensor. $^{***}p < 0.001$ by unpaired t test.

Table S4. Clinical characteristics of BBD patients **(Fig. 6A** and **6B**).

No.	Age	Clinical diagnosis
01	46	Fibroadenoma
02	29	Fibroadenoma
03	59	Mastitis
04	55	Fibroadenoma
05	49	Mastitis
06	51	Fibroadenoma
07	41	Mastitis
08	47	Fibroadenoma
09	47	Intraductal papilloma
10	17	Fibroadenoma

Table S5. Clinical characteristics of BC patients (**Fig. 6A** and **6B**).

No.	Age	Histologic diagnosis
01	55	Infiltrating carcinoma
02	69	Infiltrating carcinoma
03	51	Infiltrating carcinoma
04	67	Infiltrating carcinoma
05	56	Infiltrating carcinoma
06	51	Infiltrating carcinoma
07	63	Infiltrating carcinoma
08	49	Infiltrating carcinoma
09	49	Infiltrating carcinoma
10	63	Infiltrating carcinoma

Table S6. Clinical characteristics of non-metastatic BC patients (**Fig. 6C** and **6D**).

No.	Age	Histologic diagnosis	Stage
01	63	Infiltrating carcinoma	II
02	53	Infiltrating carcinoma	II
03	58	Infiltrating carcinoma	II
04	40	Infiltrating carcinoma	II
05	73	Infiltrating carcinoma	II
06	36	Infiltrating carcinoma	II
07	64	Infiltrating carcinoma	II
08	48	Infiltrating carcinoma	II

Table S7. Clinical characteristics of metastatic BC patients (**Fig. 6C** and **6D**).

No.	Age	Histologic diagnosis	Stage
01	58	Infiltrating carcinoma	IV
02	59	Infiltrating carcinoma	IV
03	47	Infiltrating carcinoma	III
04	65	Infiltrating carcinoma	IV
05	54	Infiltrating carcinoma	III
06	44	Infiltrating carcinoma	III
07	41	Infiltrating carcinoma	III

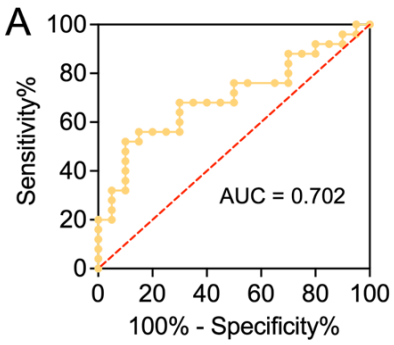

Cut-off (ng mL^{-1})	DP (%)	PPV (%)	NPV (%)	Accuracy (%)
2.74	55.56	86.67	60.00	68.89

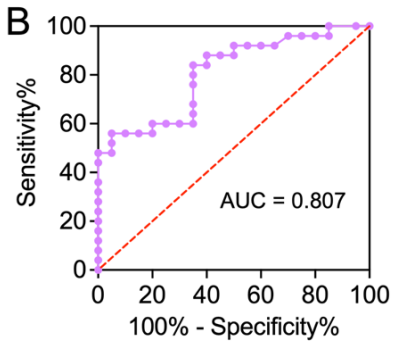

Cut-off (U mL^{-1})	DP (%)	PPV (%)	NPV (%)	Accuracy (%)
19.15	55.56	93.33	63.33	73.33

Fig. S17 ROC curves and diagnostic testing evaluation of (A) CEA and (B) CA15-3 measured by using ARCHITECT i2000SR immunoassay analyzer (Abbott, USA) for breast cancer diagnosis.

Reference

1. Jia Y, Ren X, Zhang X, Wu D, Ma H, Li Y, Wei Q. Encapsulation of Tetraphenylethylene Derivative in Liposome Vesicles as Promising Aggregation-Induced Electrochemiluminescence Emitter for Detection of Human Epidermal Growth Factor Receptor 2. Anal Chem. 2023;95:9139-9144.
2. Dervisevic M, Alba M, Adams TE, Prieto-Simon B, Voelcker NH. Electrochemical immunosensor for breast cancer biomarker detection using high-density silicon microneedle array. Biosens Bioelectron. 2021;192:113496.
3. Wang X-Y, Feng Y-G, Wang A-J, Mei L-P, Yuan P-X, Luo X, Feng J-J. A facile ratiometric electrochemical strategy for ultrasensitive monitoring HER2 using polydopamine-grafted-ferrocene/reduced graphene oxide, Au@Ag nanoshuttles and hollow Ni@PtNi yolk-shell nanocages. Sensor Actuat B: Chem. 2021;331.
4. Kuntamung K, Jakmunee J, Ounnunkad K. A label-free multiplex electrochemical biosensor for the detection of three breast cancer biomarker proteins employing dye/metal ion-loaded and antibody-conjugated polyethyleneimine-gold

nanoparticles. J Mater Chem B. 2021;9:6576-6585.
5. Wang Y, Chen S, Tian S, Wei Q, Tang D. Edge-generated N-doped carbon-supported dual-metal active sites for enhancing electrochemical immunoassay. Anal Chim Acta. 2023;1284:342006.
6. Zeng R, Li Y, Li Y, Wan Q, Huang Z, Qiu Z, Tang D. Smartphone-Based Photoelectrochemical Immunoassay with Co(9)S(8)@ZnIn(2)S(4) for Point-of-Care Diagnosis of Breast Cancer Biomarker. Research (Wash D C). 2022;2022:9831521.
7. Wang W, Han R, Chen M, Luo X. Antifouling Peptide Hydrogel Based Electrochemical Biosensors for Highly Sensitive Detection of Cancer Biomarker HER2 in Human Serum. Anal Chem. 2021;93:7355-7361.
8. Qiu M, Ren Y, Huang L, Zhu X, Liang T, Li M, Tang D. FeNC nanozyme-based electrochemical immunoassay for sensitive detection of human epidermal growth factor receptor 2. Microchim Acta. 2023;190:378.